# The role of bridging ligand in hydrogen generation by photocatalytic Ru/Pd assemblies

Bindra, Gurmeet Singh; Schulz, Martin; Paul, Avishek; Groarke, Robert; Soman, Suraj; Inglis, Jane L.; Browne, Wesley R.; Pfeffer, Michael G.; Rau, Sven; MacLean, Brian J.

*Published in:*
Dalton Transactions

*DOI:*
10.1039/c2dt30948c



*Publication date:*
2012

Dalton Transactions

Cite this: *Dalton Trans.*, 2012, **41**, 13050

www.rsc.org/dalton

PAPER

# The role of bridging ligand in hydrogen generation by photocatalytic Ru/Pd assemblies†‡

**Gurmeet Singh Bindra,[a] Martin Schulz,[a,b] Avishek Paul,[a] Robert Groarke,[a] Suraj Soman,[a] Jane L. Inglis,[a] Wesley R. Browne,[c] Michael G. Pfeffer,[d] Sven Rau,[d] Brian J. MacLean,[e] Mary T. Pryce[a] and Johannes G. Vos*[a]**

***Received 1st May 2012, Accepted 15th June 2012***
**DOI: 10.1039/c2dt30948c**



The synthesis and characterisation of two terpyridine based ruthenium/palladium heteronuclear compounds are presented. The photocatalytic behaviour of the Ru/Pd complex containing the linear 2,2′:5′,2″-terpyridine bridge (**1a**) and its analogue the non-linear 2,2′:6′,2″-terpyridine bridge (**2a**) are compared together with the respective mononuclear complexes **1** and **2**. Irradiation of **1a** with visible light (*e.g.*, 470 nm) results in the photocatalytic generation of dihydrogen gas. Photocatalysis was not observed with complex **2a** by contrast. A comparison with the photocatalytic behaviour of the precursors **1** and **2** indicates, that while for **1a** the photocatalysis is an intramolecular process, for the mononuclear precursors it is intermolecular. The photophysical and electrochemical properties of the mono- and heterobinuclear compounds are compared. Raman spectroscopy and DFT calculations indicate that there are substantial differences in the nature of the lowest energy $^3$MLCT states of **1a** and **2a**, from which the contrasting photocatalytic activities of the complexes can be understood.

## Introduction

Hydrogen is widely perceived to be one of the primary fuels of the future, in particular for the transport sector because of its exceptionally high energy-density/mass ratio. One of the most promising approaches towards the generation of hydrogen in an environmentally friendly and sustainable manner is the use of molecular photocatalysts that utilise visible light to drive proton reduction. Such systems are comprised of a light-harvesting antenna that can donate electrons to a catalytically active centre *via* a bridging ligand. Due to their exceptional photophysical and redox properties Ru(II) polypyridyl complexes are an excellent choice as the light harvesting centre[1] while Pd(II) or Pt(II) are often the metal of choice for the catalytically active centres.[2] Alternative combinations already reported are the combinations of Re/Co, Ru/Pd, Ru/Pt, Os/Rh, Ru/Rh, Pt/Co and Ir/Rh.[3] The perception that intramolecular electron transfer from the light harvesting centre to the catalytic centre *via* the bridging ligand has stimulated the search for suitable bridging ligands. However, changes to the peripheral ligand can influence the catalytic properties of the assemblies also.[2b,4]

In this contribution two new Ru(II)/Pd(II) heterobinuclear metal complexes **1a** and **2a** (Fig. 1) and their photocatalytic properties with regard to hydrogen production are reported. The complexes are based on terpyridine bridging ligands with the linear 2,2′:5′,2″-terpyridine bridge (2,5-bpp) used in **1a** and the angular 2,2′:6′,2″-terpyridine bridging moiety (2,6-bpp) in **2a**. We show here that **1a** (with the linear 2,5-bpp ligand) can catalyse the production of hydrogen while **2a** does not. In addition preliminary wavelength dependent studies on the catalytic

[a]*SRC for Solar Energy Conversion, School of Chemical Sciences, Dublin City University, Glasnevin, Dublin 9, Dublin, Ireland. E-mail: han.vos@dcu.ie*
[b]*Lehrstuhl für Pharmazeutische Radiochemie, Technische Universität München, Walther-Meißner-Str. 3, 85748 Garching, Germany*
[c]*Stratingh Institute for Chemistry, Faculty of Mathematics and Natural Sciences, University of Groningen, Nijenborgh 4, 9747 AG Groningen, The Netherlands*
[d]*Anorganische Chemie I, Universität Ulm, Albert-Einstein-Allee 11, 89081 Ulm, Germany*
[e]*Department of Chemistry, St. Francis Xavier University, Physical Sciences Building, P.O. Box 5000, Antigonish, Nova Scotia, B2G-2W5, Canada*

†Based on the presentation at Dalton Discussion No. 13, 10–12 September 2012, University of Sheffield, UK.
‡Electronic supplementary information (ESI) available: $^1$H NMR spectra, cyclic voltammetry and orbital contributions tables. See DOI: 10.1039/c2dt30948c

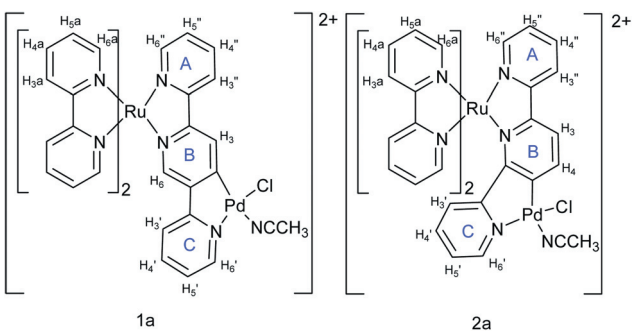


**Fig. 1** Structure of complexes $[Ru(bipy)_2(2,5\text{-bpp})Pd(CH_3CN)Cl](PF_6)_2$ (**1a**) and $[Ru(bipy)_2(2,6\text{-bpp})Pd(CH_3CN)Cl](PF_6)_2$ (**2a**). The mononuclear precursor Ru(II)-complexes are denoted **1** and **2**.

efficiency suggest that the highest efficiency may be obtained when the lowest energy $^3$MLCT states are localised on the bridging ligand.

## Results and discussion

### Synthesis

The linear 2,2′:5′,2″-terpyridine ligand was prepared through a Negishi coupling of 2,5-dibromopyridine with 2-pyridylzinc bromide using modified published procedures[5] and obtained with moderate yields. Complexes **1** and **2** were obtained in excellent yields from $[Ru(bipy)_2Cl_2]\cdot 2H_2O$. Heating **1** and **2** in alcoholic solution at reflux with $(NH_4)_2[PdCl_4]$ for several days afforded the heterodinuclear complexes **1a** and **2a** in good yield.

A key issue is the actual molecular structure of the active compounds. In Fig. 1 the Pd centre is coordinated to the bridging bpp ligand, as well as to a chlorido and an acetonitrile ligand, and elemental analysis supports this structure. However, a tetranuclear structure such as in Fig. 2 is also possible, whereby the acetonitrile is not bound to the Pd(II) centre but is solvent of crystallisation.

The $^1$H NMR spectrum of **1a** is shown in Fig. S2a, ESI.‡ The resonance at 2.06 ppm, when compared with related Pd(II) complexes, can be assigned to coordinated acetonitrile.[6] A similar assignment can be made for **2a** (Fig. S2b, ESI‡). Hence, in solution the structure is most likely to be that shown in Fig. 1. It is worth noting that the products obtained from the reaction between **1** (or **2**) and the Pd(II) precursor are insoluble in a range of solvents except upon addition of acetonitrile (*e.g.*, to acetone) when dissolution occurs. This suggests that the product obtained from this reaction may have the structure as shown in Fig. 2, but that upon addition of acetonitrile the solvent adduct is formed. For the photocatalytic and electrochemical experiments it is assumed that the molecular structure of the compounds is that shown in Fig. 1.

Steric interactions between the 2,6-bpp ligand and the bipy ligands results in the pyridine ring not coordinated to the Ru(II) centre sitting out of the plane of the other two pyridine rings (*vide infra*). $^1$H NMR spectroscopy shows that for **1**, which contains the sterically constrained 2,5-bpp ligand (Fig. S1, ESI‡), and for **1a** four sets of bipyridine multiplets (8.64–8.54, 8.15–8.07, 7.95–7.78, 7.48–7.38 ppm) were observed due to the similar chemical environment of all bipyridine ligands. In contrast, up to twelve resolved sets of signals were observed for the bipyridine ligands of **2** and **2a**, indicating the different chemical environments that these ligands are in (Fig. S2, ESI‡). The chemical shifts of the bridging ligands are similar for all complexes. Assignment of the signals observed was facilitated by deuteriation[7] of the bipy ligands (see Fig. S1 and S2, ESI‡) and by the use of $^1$H COSY NMR spectroscopy.

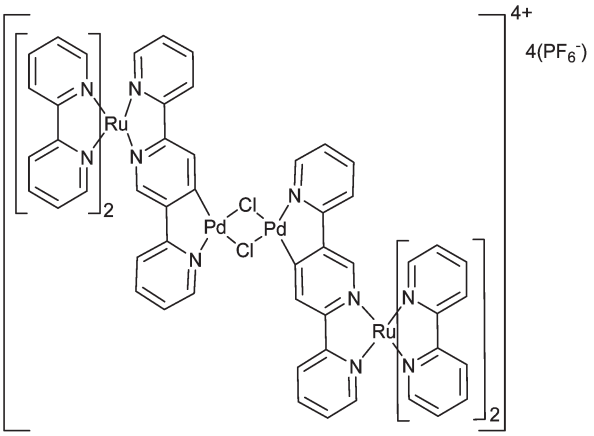


**Fig. 2** Possible structure for RuPd photocatalyst **1a** in the solid state.

### UV/Vis spectroscopic and redox properties

The spectroscopic and electrochemical properties of the compounds are shown in Table 1 and Fig. 3. The absorption and emission maxima show only minor changes upon addition of the Pd(II) centre; however, a considerable decrease in emission lifetime is observed *e.g.*, from 442 ns for **1** to 105 ns for **1a**. The decrease in emission lifetime, however, is not accompanied by a corresponding decrease in emission quantum yield, which suggests that the coordination of the palladium centre increases the rate of radiative relaxation possible through increased spin orbit coupling effects. A similar observation was made by Sakai and co-workers.[8] This also suggests that the lowest excited states are bipy based for both mono- and heterodinuclear complexes in agreement with transient Raman studies. The DFT calculations suggest however that other excited states with similar energy which are bridge based are also present (*vide infra*).

The electrochemical properties of the complexes were investigated using both CV (cyclic voltammetry) and DPV (differential pulse voltammetry) in DMF (Fig. S3, ESI‡). In acetonitrile very similar results were obtained. **1** and **2** show well-defined oxidation waves {Ru(II)/Ru(III)} and reductions assigned to ligand based reductions.

Interpretation of the cyclic voltammetry of the heterodinuclear complexes is, in contrast, not straightforward due to the observation of a number of irreversible processes (Fig. S3, ESI‡). The data obtained for **1a** and **2a** were compared with those obtained for **1**, **2** and $[(2\text{-phenylpyridine})Pd(\mu\text{-}Cl)]_2$ (**3**). Compounds **1a** and **2a** show three oxidative processes, the second wave at *ca.* 0.84 V for **1a** and at 0.78 V for **2a** is quasi reversible, while the first and third are irreversible. The irreversible processes are assigned to Pd based oxidations by comparison with **3** (Table 1). It is worth noting that the Ru(II)/(III) redox potential does not change significantly upon the coordination of Pd(II). This suggests that the energy of the ground state is largely unaffected. A number of ill-defined processes are observed at negative potentials for both **1a** and **2a**, and assignment of individual redox couples is therefore not possible. Previous studies of related ruthenium complexes have shown that a 2,5-bpp based reduction generally occurs at more positive potentials than for bipy based reductions.[9]

Of particular interest at negative potentials are the Pd(II) based reduction waves. Again a definitive assignment cannot be made, however the least negative processes at −1.67 V (**1a**) and −1.92 V (**2a**) are most likely ligand centred reductions. In compounds **1** and **2** a wave is observed at similar potentials, however assuming that this reduction is bpp based, it can be expected that this

**Table 1** UV/Vis spectroscopic and electrochemical properties of **1**, **1a**, **2** and **2a**

| | Abs./nm {$\varepsilon$ $10^4$ $M^{-1}$ $cm^{-1}$} | Em./nm {$\tau^a$/ns} | $\Phi_{Em}$ | $E_{ox}{}^b$ (V) | $E_{red}{}^b$ (V) |
|---|---|---|---|---|---|
| **1** | 455 {1.18} | 630 {442} | 0.047 | 0.83 | −1.64, −1.95, −2.16, −2.53 |
| **1a** | 463 {1.33} | 635 {105} | 0.032 | 0.73[c], 0.84, 1.02[c] | −1.43[c], −1.67, −1.88, −2.10, −2.37[d,c], −2.55[d] |
| **2** | 449 {1.88} | 627 {33} | 0.003 | 0.77 | −1.77, −1.97, −2.27 |
| **2a** | 449 {1.72} | 635 {[e]} | 0.001 | 0.66[c], 0.78, 0.93[c] | −1.76[c], −1.92, −2.10, −2.31, −2.27, −2.37[d] |
| **3** | | | | 0.70[c], 1.03[c] | −2.31[c], −2.45[c], −2.49 |

[a] By TCSPC at 293 K in de-aerated acetonitrile solution. [b] Cyclic voltammetry in DMF with 0.1 M $TBAPF_6$ *vs.* $Fc/Fc^+$ couple. Data were obtained at 263.15 K for **1a** and **2a**. [c] Peak potentials for irreversible processes. [d] Determined using differential pulse voltammetry. [e] lifetime less than instrument response (<1 ns).



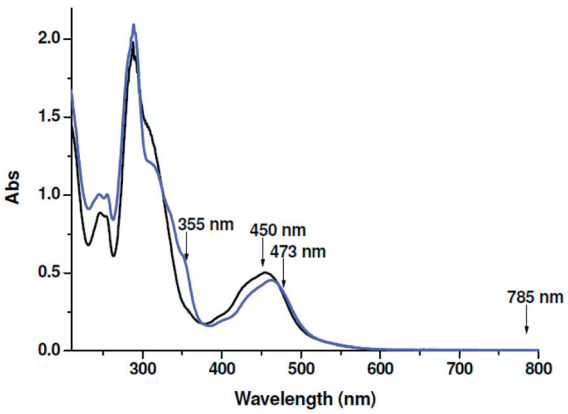


**Fig. 3** UV-Vis absorption spectra of **1** (black) and **1a** (blue). Wavelengths used to record Raman spectra are indicated.

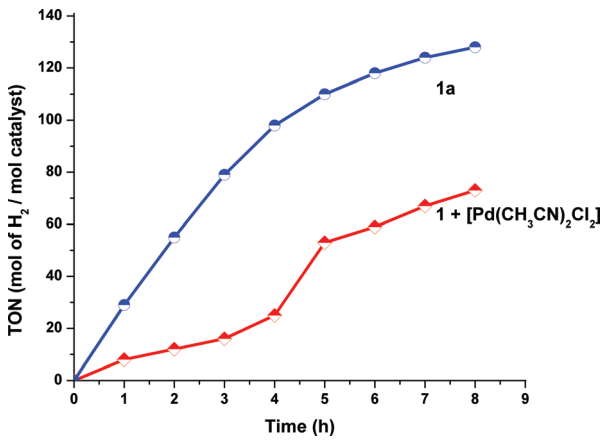


**Fig. 4** Time-dependence of the TON achieved for $H_2$ evolution in the presence of 10% water for **1a** (blue) and **1** with $[Pd(CH_3CN)_2Cl_2]$ (red).

wave will be at more negative potentials when the ligand is cyclo-metallated.

These UV/Vis spectroscopic and electrochemical data overall indicate that coordination of Pd(II) to **1** (and **2**) has only a modest effect and the photophysical properties of the ruthenium centre remain largely unchanged, albeit with a red-shift in the ππ* absorption bands of the bpp ligands to *ca.* 350 nm. The absence of a substantial change in the absorption and emission maxima and the indication from electrochemical data that the Ru(II) centred HOMO orbitals are unchanged in terms of energy suggest that the primary effect of complexation of the Pd(II) centre is to reduce the radiative lifetimes and to introduce an additional excited state deactivation channel (*e.g.*, energy or electron transfer to the palladium centre).

**Table 2** Turnover numbers (TON) for hydrogen generation

| Compounds / Water content | TON as function of water content[a] (v/v) 0% | 5% | 10% |
|---|---|---|---|
| **1a** | 0 | 108 | 130 |
| **2a** | 0 | 0 | 0 |
| **1** + $(NH_4)_2[PdCl_4]$[b] | — | 50 | 48 |
| **1** + $[Pd(CH_3CN)_2Cl_2]$[b] | — | 79 | 70 |
| **2** + $(NH_4)_2[PdCl_4]$[b] | — | 0 | 0 |
| **2** + $[Pd(CH_3CN)_2Cl_2]$[b] | — | 0 | 0 |

[a] Determined by GC after irradiation for 18 h. [b] The reaction mixture contains an equimolar mix of the mononuclear complex and Pd species $3.0 \times 10^{-5}$ M, [TEA] = 2.30 M.

## Photocatalysis

The photocatalytic properties of **1a** and **2a** were investigated in acetonitrile with the sacrificial reductant triethylamine (TEA) and compared with solutions containing the mononuclear complexes **1** or **2** and $[Pd(CH_3CN)_2Cl_2]$. As anticipated no photocatalytic water-splitting, was observed in the absence of water, however when solutions contained 5 or 10 vol% water $H_2$ was generated with turnover numbers shown in Table 2. The turnover numbers (TONs) for $H_2$ production obtained after irradiation at 470 nm for 18 h are given in Table 2. TONs of up to 130 (16 μmol after 18 h) were obtained for **1a**. The time dependence of $H_2$ evolution by **1a**, and **1** with $[Pd(CH_3CN)_2Cl_2]$, expressed as TON over an 8 h period is shown in Fig. 4. Remarkably, $H_2$ production was not observed with **2a**.

Photocatalytic hydrogen production was also observed when the catalyst was prepared by mixing **1** with $[Pd(CH_3CN)_2Cl_2]$ or $(NH_4)_2[PdCl_4]$ *in situ*; however lower TONs were obtained than for **1a** under the same conditions. Furthermore the lack of activity of the *in situ* prepared catalyst over the first 4 h of the reaction and the absence of conversion when $[Pd(CH_3CN)_2Cl_2]$ was used alone support the conclusion that the $H_2$ evolution originates from an intramolecular process in the heterodinuclear complex. Furthermore, it is clear from Fig. 4 that the activity is highest in the early stages of the reaction ($t$ < 4 h). Control

 

experiments with the mononuclear precursors **1** and **2** without Pd species present or by mixing **2a** with $[Pd(CH_3CN)_2Cl_2]$ did not show evidence of $H_2$ production.

The formation of colloids for $H_2$ generation has been discussed by several authors.[10] Since both complexes have comparable binding properties for Pd it seems unlikely that one should act as a precursor for catalytically active colloids while the other does not. Indeed given the greater steric demands that the coordination of palladium places on complex **2a**, it would be expected to be this complex that releases palladium more rapidly. This is not the case, however. The formation of a black precipitate is observed for **1**/$[Pd(CH_3CN)_2Cl_2]$ and for **1a** under catalytic conditions and suggests dissociation of the palladium. By contrast precipitates were not observed for **2a** under the same conditions. It should be noted that the standard mercury test,[11] used to identify the presence of Pd nanoparticles, has previously been found to be inappropriate for these types of complexes.[4]

The wavelength dependence of $H_2$ production by **1a** was examined (Fig. 5). A maximum TON of 130 with 10% water was obtained close to the maximum absorption (463 nm, $\varepsilon$ = 1.33 × $10^4$ $M^{-1}$ $cm^{-1}$) when irradiated at 470 nm ($\varepsilon$ = 1.28 × $10^4$ $M^{-1}$ $cm^{-1}$) for 18 h (Table 2). For other excitation wavelengths the TON decreased according to the absorption spectrum; at 520 nm ($\varepsilon$ = 0.21 × $10^4$ $M^{-1}$ $cm^{-1}$), TON = 51; at 590 nm ($\varepsilon$ = 0.03 × $10^4$ $M^{-1}$ $cm^{-1}$), TON = 5; and at 630 nm ($\varepsilon$ = 0 $M^{-1}$ $cm^{-1}$), TON = 0. When differences in molar absorptivity are taken into account, the efficiency is higher when excitation is at longer wavelengths, *i.e.* efficiency is not constant over the visible spectrum.

For heterogeneous photocatalytic hydrogen production with graphitic $C_3N_4$ (g-$C_3N_4$) the catalytic activity follows the absorption spectrum strictly.[12,13] However, Rau and co-workers, have observed wavelength dependence for the efficiency of the complex $[Ru(tbbpy)_2(tpphz)PdCl_2](PF_6)_2$ where the catalytic activity did not follow the absorption spectrum strictly.[14] The origin of this effect could lie in the involvement of a one electron reduced intermediate state; *i.e.* excitation of **1a** is followed either by relaxation to **1a** or reduction of the excited complex by TEA to yield **1a**$^-$. The absorption spectrum of this species would be expected to be substantially different and hence the second excitation, if rate limiting, will depend not on the spectrum of **1a** but on the one electron reduced **1a**$^-$. Alternatively, recent studies on related iridium compounds[3j] indicate that the efficiency of hydrogen formation may depend on the nature of the excited state populated as also suggested in ref. 14. These latter investigations on a tpphz based photocatalyst utilised laser excitation sources with a constant photon flux. This is technically not easily accomplished with LED excitations. More detailed studies into these observations are necessary especially with more accurate excitation sources in order to obtain more detailed information.

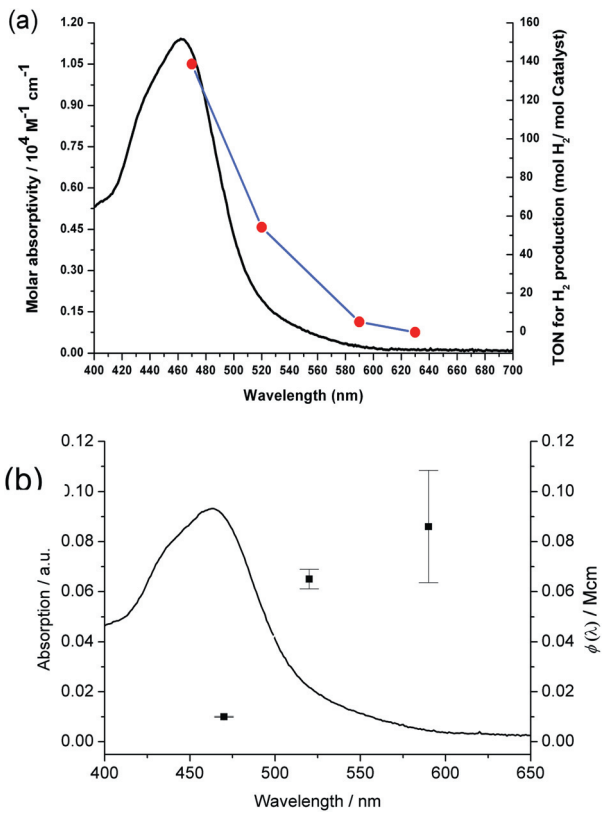


**Fig. 5** (a) Wavelength dependence of photocatalytic hydrogen generation and (b) the efficiency spectrum $\Phi(\lambda)$ for complex **1a**. For conditions see the Experimental section.

## Raman spectroscopy

Resonance Raman spectroscopy has proven to be a powerful tool in the association of electronic absorption bands with individual ligands, in particular metal to ligand change transfer bands in Ru(II) polypyridyl complexes.[15] In addition the use of nanosecond pulsed lasers can provide information regarding the nature of the lowest electronically excited states.[16] This technique was therefore used to further investigate the electronic properties of the hydrogen producing compound **1a** and its precursor **1**. The excitation wavelengths used to record these spectra are shown in Fig. 3. The (non-resonant) Raman spectra of **1** and **1a** are shown in Fig. 6. For both compounds Raman bands typical of 2,2-bipyridyl ligands are present at 1604, 1556, 1487, 1317, 1274, 1173, 1108, 1039, 1028, 766, 662 and 646 $cm^{-1}$,[17] however, in each case additional bands were observed that can be ascribed to the 2,5-bpp and orthometallated 2,5-bpp$^-$ ligands, respectively. For **1**, bands assignable to the 2,5-bpp ligand are evident at 1604, 1590, 1505, 1474, 1435, 1377, 1324(sh), 1302, 1234, 1030, 991, 805, 678 and 649 $cm^{-1}$. For **1a** the bands are shifted

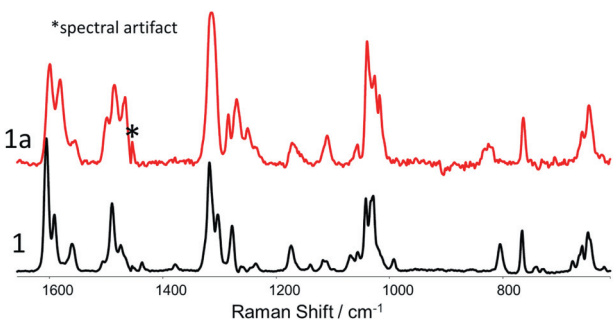


**Fig. 6** (Non-resonant) Raman spectra of **1** and **1a** (photocatalyst) in the solid state ($\lambda_{exc}$ 785 nm).

compared with **1** as expected due to the deprotonation of the 2,5-bpp ligand and are at 1599, 1581, 1499, 1466, 1312, 1283, 1250, 1109, 1027 and 1016 and 647 $cm^{-1}$. Of particular interest, with regard to the discussion of the resonance Raman data below, are the bands at around 1490 $cm^{-1}$, as the bands of the 2,5-bpp and (−H)2,5-bpp$^-$ ligands are of comparable intensity to that of the bipy ligands. Importantly, however, it is clear from the non-resonant Raman spectra that vibrational modes of the 2,5-bpp ligand can easily be distinguished from those of the bipy ligands and that the vibrational modes of the bpp ligand change considerably upon orthometallation by the palladium.

The electronic absorption bands observed in **1** and **1a** at 355 nm are absent in $[Ru(bipy)_3]^{2+}$ and are therefore tentatively assigned as 2,5-bpp and 2.5-bpp$^-$ π–π* transitions, respectively. This assignment is confirmed by the resonance Raman spectra recorded at 355 nm (Fig. 7 and 8) in which bands assignable to the 2,5-bpp and 2,5-bpp$^-$ ligands are observed and the well-known bipy modes are completely absent.

Of particular interest in the present study is the nature and localisation of the $^1$MLCT transitions present in the visible region since they are expected to be heavily involved in the photocatalytic process. Although the relatively strong emission observed for both **1** and **1a** precludes acquisition of spectra at the longest wavelength absorption available (*e.g.*, 532 nm), good quality resonance enhanced Raman spectra could be obtained at 450 and 473 nm, which represent the maximum and red shoulder of the $^1$MLCT absorption manifolds. For **1**, bands assignable to a bipy based ($^1MLCT_{bipy} \leftarrow GS$) (where GS is ground state) absorption could be observed at 1605, 1560, 1490 $cm^{-1}$ with no significant resonant enhancement of the 2,5-bpp modes. This suggests that for this compound the red side of the MLCT manifold is dominated by bipy based transitions. In stark contrast, for **1a** excitation at both 450 and 473 nm showed strong contributions from modes originating from both the bipy ligands and the 2,5-bpp$^-$ ligand, with the 2,5-bpp$^-$ modes dominating the Raman spectrum when excitation was at the red edge of the absorption manifold (*i.e.* 473 nm), Fig. 8. This indicates that for

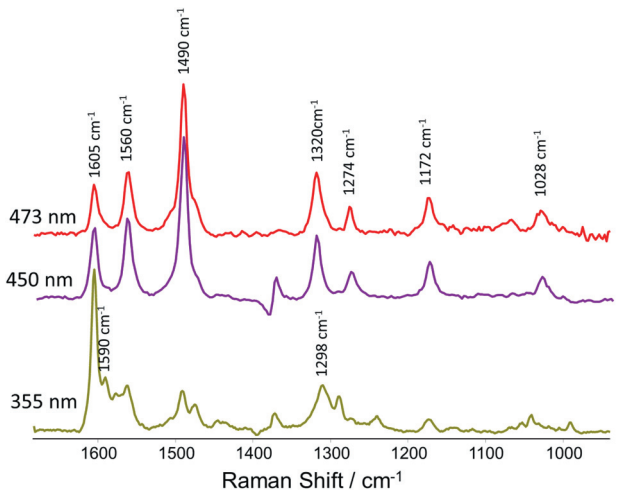


**Fig. 7** Resonance Raman spectra of **1** in $CH_3CN$ (solvent subtracted) at 355, 450 and 473 nm.

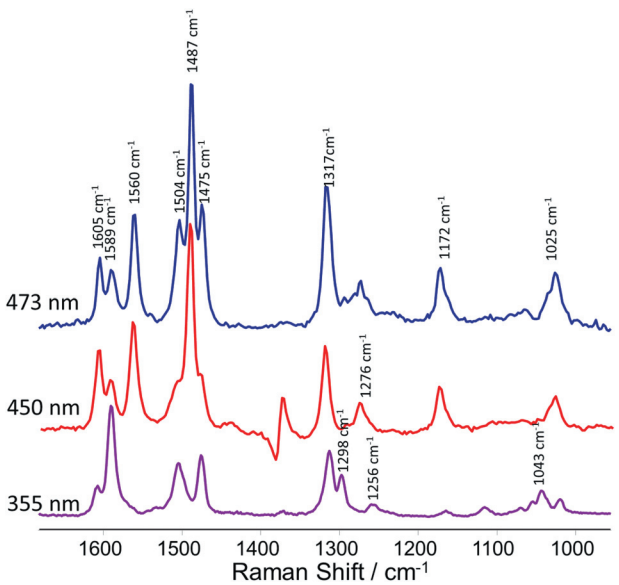


**Fig. 8** Resonance Raman spectra of **1a** in $CH_3CN$ (solvent subtracted) at 355, 450 and 473 nm.

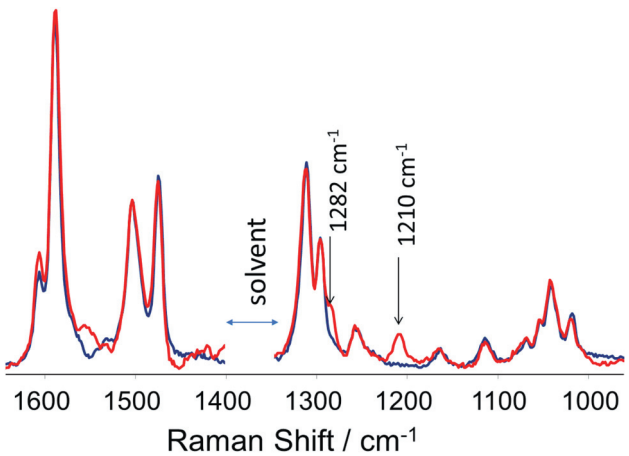


**Fig. 9** Resonance Raman spectra of **1a** in $CH_3CN$ (solvent subtracted) at 355 nm with (blue) continuous wave (CW) and (red) pulsed excitation. The characteristic modes of the bipy anion radical are observed at 1282 and 1210 $cm^{-1}$.

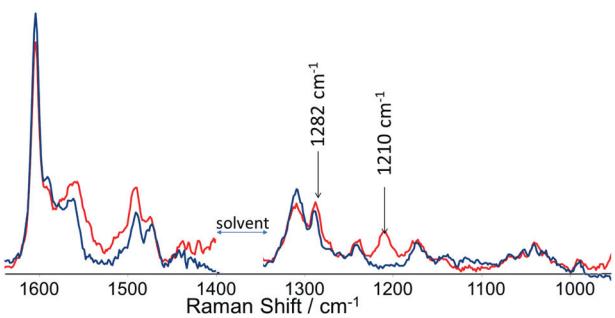


**Fig. 10** Resonance Raman spectra of **1** in $CH_3CN$ (solvent subtracted) at 355 nm with (blue) CW and (red) pulsed excitation. The characteristic modes of the bipy anion radical are observed at 1282 and 1210 $cm^{-1}$.

**1a**, $^1$MLCT$_{bpp^-}$ ← GS transitions are generally lower or equal in energy to the $^1$MLCT$_{bipy}$ ← GS transitions.

Resonance Raman spectra obtained with pulsed rather than continuous wave excitation at 355 nm can potentially provide further information as to the nature of the lowest $^3$MLCT excited state as shown in Fig. 9 and 10. For **1** and **1a** the strong resonance enhancement of Raman scattering from the 2,5-bpp ligand (*vide supra*) means that the spectra obtained with pulsed excitation are dominated by ground state modes. Nevertheless, comparison of spectra obtained at 355 nm using CW and pulsed excitation shows the appearance of bands characteristic of the bipy anion radical[17] and hence although significant population of a 2,5-bpp based $^3$MLCT excited cannot be excluded, it is clear that the lowest $^3$MLCT manifold also involves bipy based $^3$MLCT states.

### Computational studies

The data described above confirm that the Ru/Pd complexes **1a** and **2a** have different catalytic behaviours. High level DFT calculations were carried out to further investigate the electronic properties of the complexes. The geometries of complexes **1**, **1a**, **2** and **2a** were calculated as minimum structures and the IEF-PCM formalism was used to model the influence of the solvent acetonitrile (for details see Experimental part). Although the singlet states of Ru(II) polypyridyl complexes can be reasonably well described by the popular B3LYP functional (20% Hartree–Fock exchange) it failed for the calculation of the lowest energy triplet states. We thus tested three τ-dependent functionals with varying Hartree–Fock contributions, namely, M06-L (0%), M06 (27%) and M06-HF (100%).[18] M06-L and M06 were successfully applied for the modelling of the lowest energy triplet state of **1a** and **2a** but M06-HF failed. M06 was then chosen for the re-calculation of the singlet states and also for the modelling of the singly reduced doublet states, since the M06 results give a more delocalised picture. It is worth noting that the calculations are sensitive to the chosen functional and hence great care must be taken. A comparison of selected calculated and experimental bond lengths is given in Table 3 and the structures of the calculated complexes are given in Fig. 11. The differences due to the metallation and the different structures of the bridging ligands were studied by comparing the calculated geometric parameters of the dinuclear complexes **1a** and **2a** with each other as well as with their mononuclear counterparts. In agreement with the UV/Vis absorption data, the 2,5-bpp ligand of **1a** can be considered as a pyridyl substituted bipyridine with electronic communication between the two parts. In contrast the 2,6-bpp ligand can be viewed as a bipyridine in which there is little communication with its pyridyl substituent. This is due to the geometric distortions discussed above and is apparent in the results of the calculations (Fig. 11). Delocalisation of bridge based molecular orbitals is not hindered by the metallation of the central pyridine ring. Comparison of the M06 geometries of **1** and **1a** as well as **2** and **2a** revealed no induced alteration of the bridging ligand bond lengths on addition of palladium. Analysis of the charges on each atom also shows that the presence of palladium does not result in changes except for the metallated carbon atom having a more negative value. In summary, the charge of the cyclo-metallated carbon is localised and the electronic properties of the bridge remain mainly unchanged. The only exception is the metallation induced planarity of the 2,5-bpp-bridge of **1a** that allows for greater delocalisation of bridge-based orbitals and hence a red shift of transitions that have significant contributions from the bpp ligand. The geometric distortion of the 2,6-bpp-bridge remains in the metallated complex **2a** and hence prevents substantial delocalisation of bridge based orbitals. The out of plane nature of the 2,6-bpp bridge leads to larger Ru–N bond lengths varying between 220 pm for the Ru–N(ring-A) and 206 pm Ru–N(bipy).

**Table 3** Comparison of experimental values with the M06 geometries of singlet-**1a** and singlet-**2a**

| Bond lengths [pm] | **1a** (M06) | **2a** (M06) | Exp | Ref. |
|---|---|---|---|---|
| Ru–N | 208[a] | 211[a] | 205[a] | 19 |
| Pd–Cl | 235 | 235 | 236 | 20 |
| Pd–N | 208 | 207 | 202 | 20 |
| Pd–ACN | 214 | 214 | 214 | 20 |
| Pd–C | 198 | 198 | 199 | 20 |

The angular nature of the 2,6-bpp bridge leads to larger Ru–N(py) bond lengths.[a] Average values.

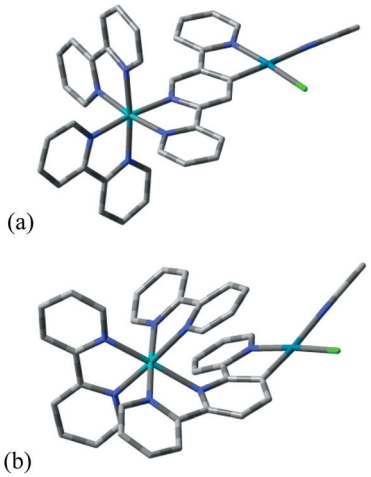


**Fig. 11** Presentation of the optimised structures of (a) singlet-**1a** and (b) singlet-**2a**.

The spatial localisation of the molecular orbitals was calculated through a population analysis. Their localisation on a certain part of the molecule is expressed as per cent contribution and given in Tables S1–S6, ESI.‡ The calculations indicate that the localisation of the SOMOs in the triplet states of **1a** and **2a** differ from the localisation of the LUMO of their singlet states. However, the LUMO of the singlet state and the SOMO of the mono-reduced doublet state have a similar spatial localisation.

Analysis of the frontier orbitals of the singlet ground state of $^1$**1a** and $^1$**2a** shows the expected electronic configuration. The three highest energy occupied orbitals (HOMO-2–HOMO) are localised on the Ru(II) centre (Fig. 12 and Tables S1–S6, ESI‡). The LUMO is a bridge based orbital while L+1 and L+2 are localised on the bipy ligands. This is in agreement with resonance Raman results that show electronic transitions to the bpp ligand at lower energy than the electronic transitions to the bipy

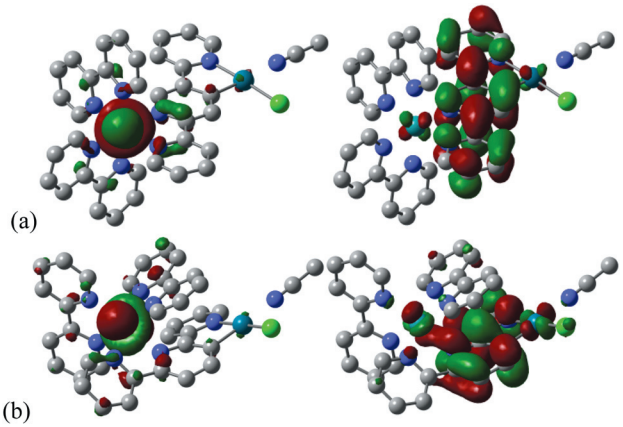


**Fig. 12** Presentation of selected frontier orbitals. (a) $^{1}$**1a** HOMO and LUMO and (b) $^{1}$**2a** HOMO and LUMO.

ligands. The lowest energy triplet states are assumed to be the emissive state and were calculated as fully relaxed minimum structures, thus the energy difference between the triplet and the singlet state should match the $E^{0-0}$ emission energy. Indeed, the M06 SCF energy difference (ΔSCF = SCF (Triplet) − SCF (Singlet)) for **1a** is 15 481 $cm^{-1}$ (646 nm), which is only a slightly longer wavelength than the actual emission maximum, $\lambda_{em}$ = 15 748 $cm^{-1}$ (635 nm). The M06 ΔSCF energy of **2a** is 10 633 $cm^{-1}$, which is much lower than the experimentally determined emission (Table 1), which precludes a detailed comparison between theory and experiment in this case.

Analysis of the localisation of the two unpaired electrons of $^{3}$**1a** and $^{3}$**2a** reveals several interesting differences. The highest energy singly occupied molecular orbital (SOMO) of $^{3}$**1a** is located on the bridge while for $^{3}$**2a** it is localised on the ruthenium centre (Fig. 12 and ESI‡). The SOMO-1 of $^{3}$**1a** and $^{3}$**2a** are both delocalised on the Pd centre and the bridging ligand. These results are surprising as it would be expected that the triplet state SOMO (of highest energy) would resemble the singlet state LUMO. It is furthermore surprising that the ruthenium centre of **1a** makes only negligible contributions to the SOMOs. The one electron reduced complexes are possible candidates for the resting state during the catalysis and may be formed *via* excitation followed by reduction from the sacrificial donor or direct one electron reduction in an electrochemical experiment. We modelled the minimum structure of the species $^{2}$**1a** and $^{2}$**2a** having a net charge of +1 and a multiplicity of 2. Both, $^{2}$**1a** and $^{2}$**2a** were calculated with the M06 functional showing a delocalisation of the unpaired electron over the whole bridge for $^{2}$**1a** and a delocalisation over the central pyridine ring and the Pd-bound pyridine ring for $^{2}$**2a** (Tables S5 and S6, ESI‡). This suggests that the first reduction is indeed a bridge based process as discussed above.

## Conclusions

In the present contribution, the importance of the structure of the bridging ligand to the effectiveness of heterodinuclear Ru/Pd complexes is demonstrated as is the potential of a system in which an intramolecular approach is taken with regard to combining a light harvesting component and a catalyst within the same molecule. This approach contrasts with the more widely used approach where these functions are carried out by distinct components.

In the present study the photocatalytic ability of two structurally and electronically similar complexes are shown to be very different and that the activity of **1a** is not due to the formation of nanoparticles or other palladium species. However, the nature of the actual catalytically active species remains elusive. The origin of the differences in catalytic ability of **1a** and **2a** may be related to the localisation of the LUMO since the first step in the catalytic cycle involves the formation of a one electron reduced complex. In **1a** the LUMO is mainly based on the bridge according to DFT calculations and furthermore the triplet excited state is based on the bridging ligand with only a minor contribution on the Ru centre. By contrast for $^{3}$**2a** this orbital is mostly based on the bipy ligands and the Ru centre. This latter arrangement is not as favourable for electron transfer as that observed for **1a**. Although excited state lifetimes do not correlate with hydrogen production the short excited state lifetime of **2a** may also be a possible reason for the absence of catalytic activity.[3g]

Future studies will focus on the preparation of less labile complexes, the use of less corrosive sacrificial agents or ultimately their elimination by the developing surface bound assemblies.

## Experimental

Reagents for synthesis were purchased as reagent grade and were used without further purification. 2,2′:6′,2″-terpyridine (2,6-bpp) was obtained commercially and used as received.

### Synthesis and characterisation

2,2′:5′,2″-terpyridine (2,5-bpp) was synthesised using the procedure of Kozhevnikov *et al.* with modifications.[5] $Pd(PPh_3)_4$ (0.3 g, 0.26 mmol) and 2,5-dibromopyridine (1 g, 4.22 mmol) were added under a nitrogen atmosphere to a dried two neck round bottom flask. The mixture was cooled to 0 °C in an ice bath and a 0.5 M solution of 2-pyridylzinc bromide in tetrahydrofuran (19.5 $cm^3$, 9.75 mmol) was added *via* syringe. The temperature was kept constant at 0 °C during addition. Subsequently the reaction mixture was stirred for 12 h at room temperature under a nitrogen atmosphere and a white precipitate formed. The reaction mixture was poured onto 200 $cm^3$ of a saturated aqueous solution of EDTA and $Na_2CO_3$ and stirred until the precipitate dissolved and a yellow precipitate formed. The aqueous solution and the precipitate were extracted with dichloromethane and the combined organic phase was dried over $MgSO_4$. Removal of the solvent *in vacuo* yielded the crude product which was purified by column chromatography (neutral alumina, hexane–ethyl acetate (9.5 : 0.5 v/v), TLC: $R_f$ = 0.15). Yield: 0.5 g (51%). $^{1}$H-NMR (DMSO-$d_6$, 400 MHz): $\delta$ = 9.40 (d, $J$ = 2.4 Hz, 1H, $H_6$), 8.74 (m, 2H, $H_{6'}$, $H_{6''}$), 8.62 (dd, $J$ = 8.4 Hz, $J$ = 2.0 Hz, 1H, $H_4$), 8.52 (d, $J$ = 8.4 Hz, 1H, $H_3$), 8.47 (d, $J$ = 7.8 Hz, 1H, $H_{3''}$), 8.15 (d, $J$ = 8.1 Hz, 1H, $H_{3'}$), 7.98 (m, 2H, $H_{4'}$, $H_{4''}$), 7.48 (m, 2H, $H_{5'}$, $H_{5''}$).

$[Ru(bipy)_2(2,5\text{-bpp})](PF_6)_2 \cdot 0.5(CH_3)_2CO$ (**1**): $[Ru(bipy)_2Cl_2] \cdot 2H_2O$ (0.339 g, 0.65 mmol) dissolved in 5 $cm^3$ of ethanol was

 

added drop-wise to a solution of 2,2′:5′,2″-terpyridine (0.152 g, 0.65 mmol) in 10 $cm^3$ of ethanol–water (3 : 1 v/v). The reaction mixture was heated at reflux for 8 h. Subsequently, the mixture was allowed to cool to room temperature and the solvent was removed *in vacuo*. The residue was precipitated in saturated aqueous solution of $NH_4PF_6$ followed by filtration of the product, which was then washed with 10 $cm^3$ of diethyl ether. Recrystallisation from acetone–water (3 : 1 v/v) afforded a red solid. Yield: 0.576 g, 92%. Anal. Calcd for $C_{35}H_{27}F_{12}N_7P_2Ru{\cdot}0.5\ (CH_3)_2CO$ (965.67): C, 45.39; H, 3.13; N, 10.15%. Found: C, 45.06; H, 2.95; N, 9.88%. $^1$H-NMR (acetonitrile-$d_3$, 400 MHz): $\delta$ = 8.64–8.54 (m, 4H, bipy $H_{3a}$), 8.60–8.58 (m, 2H, $H_3$, $H_4$), 8.54–8.52 (m, 2H, $H_{3''}$, $H_{6'}$), 8.30 (s, 1H, $H_6$), 8.15–8.07 (m, 4H, bipy $H_{4a}$), 8.07 (t, 1H, $J$ = 8.0 Hz, $H_{4''}$), 7.95–7.78 (m, 4H, bipy $H_{6a}$), 7.83 (t, 1H, $J$ = 7.8 Hz, $H_{4'}$), 7.75 (d, 1H, $J$ = 5.6 Hz, $H_{6''}$), 7.67 (d, 1H, $J$ = 7.6 Hz, $H_{3'}$), 7.48–7.38 (m, 4H, bipy $H_{5a}$), 7.41 (m, 1H, $H_{5''}$), 7.36 (m, 1H, $H_{5'}$).

$[Ru(bipy)_2(2,5\text{-bpp})Pd(CH_3CN)Cl](PF_6)_2$ (**1a**): $[Ru(bipy)_2(2,5\text{-bpp})](PF_6)_2$ (0.100 mg, 0.11 mmol) was dissolved in 5 $cm^3$ of methanol and added drop wise to a solution of $(NH_4)_2PdCl_4$ (0.027 g, 0.10 mmol) in 10 $cm^3$ of methanol. The reaction mixture was heated at reflux for 48 h. Subsequently the mixture was allowed to cool to room temperature. The product was precipitated by addition of 20 $cm^3$ of *n*-hexane. After filtration and washing with 10 ml of diethyl ether the red solid was recrystallised from acetone–acetonitrile (1 : 1 v/v). Yield: 0.100 g, 84%. Anal. Calcd for $C_{37}H_{29}ClF_{12}N_8P_2PdRu{\cdot}$(1118.55): C, 39.73; H, 2.61; N, 10.02%. Found: C, 39.49; H, 2.82; N, 10.04%. $^1$H-NMR (acetonitrile-$d_3$, 400 MHz): $\delta$ = 9.51 (d, $J$ = 6.0 Hz, 1H, $H_{6'}$), 9.13 (s, 1H, $H_3$), 8.64–8.54 (m, 4H, bipy $H_{3a}$), 8.45 (d, $J$ = 8.4 Hz, 1H, $H_{3''}$), 8.15–8.07 (m, 4H, bipy $H_{4a}$), 8.01 (m, 1H, $H_{4''}$), 7.95–7.78 (m, 4H, bipy $H_{6a}$), 7.86 (m, 1H, $H_{4'}$), 7.67 (d, $J$ = 5.6 Hz, 1H, $H_{6''}$), 7.46 (s, 1H, $H_6$), 7.48–7.38 (m, 4H, bipy $H_{5a}$), 7.39 (m, 1H, $H_{5'}$), 7.34 (m, 1H, $H_{5''}$), 7.18 (d, $J$ = 7.6 Hz, $H_{3'}$), 2.06 (s, 3H, $CH_3CN$).

$[Ru(bipy)_2(2,6\text{-bpp})](PF_6)_2{\cdot}2H_2O$ (**2**): $[Ru(bipy)_2Cl_2]{\cdot}2H_2O$ (0.500 g, 0.96 mmol) dissolved in 6 $cm^3$ ethanol was added drop-wise to a solution of 2,2′;6′,2″-terpyridine (0.224 g, 0.96 mmol) in 40 $cm^3$ ethanol–water (3 : 1). The reaction mixture was heated at reflux for 6 h. Subsequently, the mixture was allowed to cool to room temperature and the solvent was removed *in vacuo*. The residue was precipitated in saturated aqueous solution of $NH_4PF_6$ followed by filtration of the product, which was then washed with 10 $cm^3$ of diethyl ether. Recrystallisation from acetone–water (3 : 1 v/v) afforded a red solid. Yield: 0.510 g, 54%. Anal. Calcd for $C_{35}H_{27}F_{12}N_7P_2Ru{\cdot}2H_2O$: C, 43.22; H, 3.21; N, 10.08%. Found: C, 43.15; H, 2.82; N, 9.99% $^1$H-NMR (acetonitrile-$d_3$, 400 MHz): $\delta$ = 8.75 (br s, 1H, bipy $H_{3a}$), 8.63 (m, 2H, $H_5$, $H_{3''}$), 8.48 (d, 1H, $J$ = 7.5 Hz, bipy $H_{3a}$), 8.42–8.39 (m, 2H, bipy $H_{3a}$), 8.17–8.07 (m, 6H, $H_4$, $H_{4''}$, $H_{3'}$, bipy $H_{4a}$ (3H)), 7.96 (t, 1H, $J$ = 7.8 Hz, bipy $H_{4a}$), 7.67 (d, 1H, $J$ = 6.0 Hz, bipy $H_{6a}$), 7.62 (t, 1H, $J$ = 7.5 Hz, bipy $H_{5a}$), 7.58–7.53 (m, 2H, $H_{6''}$, bpy $H_{6a}$ (1H)), 7.41–7.28 (m, 5H, $H_3$, $H_{5''}$, $H_{5'}$, bipy $H_{6a}$ (1H), bipy $H_{5a}$ (1H)), 7.21 (t, 1H, $J$ = 7.6 Hz, bipy $H_{5a}$), 6.99 (t, 1H, $J$ = 7.5 Hz, $H_{4'}$), 6.88 (d, 1H, $J$ = 7.6 Hz, bipy $H_{6a}$), 6.85–6.76 (m, 2H, $H_{6'}$, bipy $H_{5a}$ (1H)).

$[Ru(bipy)_2(2,6\text{-bpp})Pd(CH_3CN)Cl](PF_6)_2H_2O$ (**2a**): $[Ru(bipy)_2(2,6\text{-bpp})](PF_6)_2$ (0.102 g, 0.11 mmol) dissolved in 5 $cm^3$ of methanol was added drop-wise to a solution of $(NH_4)_2[PdCl_4]$ (0.029 g, 0.11 mmol) in 10 $cm^3$ of methanol. The reaction mixture was heated at reflux for 72 h. Subsequently the mixture was allowed to cool to room temperature. The product was precipitated by addition of 20 $cm^3$ of *n*-hexane. After filtration and washing with 10 $cm^3$ of diethyl ether a red solid was recrystallised from acetone–acetonitrile (1 : 1 v/v). Yield: 0.058 g, 50%. Anal. Calcd for $C_{37}H_{29}ClF_{12}N_8P_2PdRu{\cdot}H_2O$: (1136.55): C, 39.10; H, 2.75; N, 9.86%. Found: C, 38.96; H, 2.49; N, 9.84%. $^1$H-NMR (acetonitrile-$d_3$, 400 MHz): $\delta$ = 9.12 (br s, 1H, $H_{6'}$), 9.01 (br s, 1H, bipy $H_{3a}$), 8.75 (d, 1H, $J$ = 7.5 Hz, bipy $H_{3a}$), 8.66 (d, 1H, $J$ = 7.5 Hz, bipy $H_{3a}$), 8.42 (d, 1H, $J$ = 7.8 Hz, $H_{3''}$), 8.40 (d, 1H, $J$ = 7.5 Hz, bipy $H_{3a}$), 8.24 (ddd, 1H, $J$ = 7.5 Hz, $J$ = 1.5 Hz, bipy $H_{4a}$), 8.12–8.00 (m, 4H, $H_{4''}$, bipy $H_{4a}$), 7.93 (d, 1H, $J$ = 7.5 Hz, $H_4$), 7.88 (d, 1H, $J$ = 7.6 Hz, bipy $H_{6a}$), 7.80 (d, 1H, $J$ = 7.7 Hz, $H_{3'}$), 7.70 (d, 1H, $J$ = 7.5 Hz, $H_3$), 7.69–7.59 (m, 3H, bipy $H_{6a}$), 7.55 (d, 1H, $J$ = 7.5 Hz, bipy $H_{5a}$), 7.50 (t, 1H, $J$ = 7.8 Hz, $H_{4'}$), 7.46 (d, 1H, $J$ = 7.8 Hz, $H_{6''}$), 7.29 (t, 1H, $J$ = 7.5 Hz, bipy $H_{5a}$), 7.27 (t, 1H, $J$ = 7.8 Hz, $H_{5''}$), 7.18 (t, 1H, $J$ = 7.5 Hz, bipy $H_{5a}$), 7.09 (t, 1H, $J$ = 7.4 Hz, bipy $H_{5a}$), 7.02 (t, 1H, $J$ = 7.8 Hz, $H_{5'}$), 2.07 (s, 3H, $CH_3CN$).

NMR spectra were recorded on a Bruker Advance 400 spectrometer and referenced to the solvent signal. Elemental analysis was carried out on an Exador Analytical CE440 by the Microanalytical Department of the University College Dublin. UV/Vis absorption spectra were recorded on Varian Cary 50 spectrophotometer at 20 ± 1 °C in a 1 cm pathlength quartz cuvette. Acetonitrile for spectrophotometric measurements was purchased from Aldrich in spectrophotometric grade and used as received. Electrochemical data were obtained by cyclic voltammetry and differential pulse voltammetry using a either a two-neck, V-shaped cell or a three-neck cell equipped with a Luggin capillary. Data were collected using a Ag wire quasi-reference electrode with ferrocene added as an internal reference at the end of each experiment ($E^{o'}_{Fc/Fc+}$ = 0.652 V); a Pt wire served as counter electrode. Potentials were corrected with iR compensation during data collection. Complexes were dissolved and de-aerated with UHP-grade argon in anhydrous DMF/0.1 M $Bu_4NPF_6$.

Emission and excitation spectra were obtained on a Perkin Elmer LS 50B at 20 ± 1 °C. Quantum yields were obtained from de-aerated acetonitrile solutions with [ruthenium(II)-tris(2,2′-bipyridine)] dichloride in water as a standard. Excited-state lifetimes were measured by time-correlated single photon counting on an Edinburgh Analytical Instruments TCSPC instrument (at 293 K) in de-aerated acetonitrile solution (freeze–pump–thaw triple sequence). Samples were excited with a LED at 360 nm. Raman spectra at 785 nm excitation were recorded using a Perkin Elmer Raman station. Continuous wave Raman Spectra at 355 nm (10 mW, Cobolt lasers), 450 nm (50 mW, Power technology) and 473 nm (75 mW, Cobolt lasers) were recorded using a 180° backscattering arrangement as described previously.[21] Raman scattering was focused into a Shamrock 303i spectrograph and dispersed with either a 500 nm blaze 1800 l $mm^{-1}$ or 400 blaze 2400 l $mm^{-1}$ grating onto an iDus-BU2 CCD camera (Andor technology) cooled at −60 °C. Transient Raman spectra were recorded using the same system as for CW Raman studies except that a frequency tripled Nd-YAG laser (355 nm, 6 ns FWHM, between 0.5 and 4 mJ per pulse, operating at 10 Hz, Innolas Spitlight 200). UV/Vis absorption spectra of samples

before and after measurements were recorded to verify that photo-decomposition did not occur during the recording of Raman spectra.

### Calculations

All calculations were carried out with the Gaussian 09 program suite.[22] The compounds **1**, **1a**, **2** and **2a** were optimized using the M06 functional. The MWB28[23] basis with an effective core potential was used for the heavy Ru and Pd atoms while 6-31G (d) was used for the remainder. Tight convergence criteria were applied for the geometry optimization process and local minima were confirmed by a frequency calculation. All calculations were carried out in the presence of a solvent sphere, which was modelled by the IEF-PCM[24] method in acetonitrile ($\varepsilon$ = 35.688000). Orbital contributions were calculated by a Mulliken population analysis and evaluated using GaussSum.[25]

### Photocatalysis

All manipulations were carried out under strictly anaerobic inert conditions. Acetonitrile was dried over calcium hydride and triethylamine over sodium according to common procedures and freshly distilled under nitrogen prior to use. Photocatalytic hydrogen production experiments were carried out using a home-built air-cooled apparatus (at 22 °C) under constant irradiation (LED 470 nm) of the sample. For the photocatalysis experiments 2 $cm^3$ of the sample solution were added to GC vials (total volume 5 $cm^3$, diameter 13 mm, 3 $cm^3$ headspace) in the dark and under a stream of nitrogen. The vials were closed with gas-tight septum caps. A typical sample solution was prepared by mixing 0.65 $cm^3$ of a $1.8 \times 10^{-4}$ M Ru/Pd complex in acetonitrile, 0.6 ml of triethylamine, 0.0–0.2 ml (0–10 vol%) of thoroughly degassed water and 0.55–0.75 ml of anhydrous acetonitrile. Subsequently, the GC vials were irradiated at 470 nm using an LED for 18 h. After irradiation, 20 µl samples were drawn from the headspace with a gas tight syringe (50 µl, SGE Analytical Science) and determined by GC, a Varian CP3800 chromatograph, with a thermal conductivity detector and a CP7536 Plot Fused Silica 25 MX 0.32 MMID column (length 25 m, layer thickness 30 µm) with nitrogen carrier gas (purity 99.999%). The GC was calibrated using 100% hydrogen gas. The obtained signal (retention time for $H_2$ = 1.58 min) was plotted against the calibration curve and multiplied accordingly to determine the total amount of hydrogen in the headspace. The LED-torch consists of a stick-shaped printed board (19 × 1 cm) with 30 blue LEDs (Kingbright, type L-7113PBC-G, 470 ± 20 nm) with a luminous efficiency of 2000 mcd per LED. LEDs are soldered closely on front and backside in a range of 9 cm. The torch was then placed within the home built reactor. The utilised LED excitation sources have comparable but different light intensities measured in candela, however the candela unit is not linear but has to be referenced to the CIE eye sensitivity function, $V(\lambda)$. This sensitivity function has a nearly Gaussian distribution with maximum sensitivity at 555 nm and steep tails to approximately 370 nm and 760 nm. As a consequence the photon flux of a 470 nm LED and a 520 nm LED with similar candela strength is different [International Commission on Illumination (usually abbreviated CIE for its French name, Commission Internationale de l'éclairage), 1978]. For wavelength dependent catalysis the GC vials containing the catalytic solution were irradiated with High Power LEDs with a diameter of 10 mm and constantly cooled to room temperature as described above. The manufacturer's data of the LEDs used are as follows: 470 nm LED: $I$ = 5 lumen, 20 000 mcd; 520 nm LED: $I$ = 15 lumen, 50 000 mcd; 590 nm LED: $I$ = 8 lumen, 32 000 mcd; 630 nm LED: $I$ = 9 lumen, 20 000 mcd. Analysis of the catalytic activity by GC was performed as described above.

## Acknowledgements

This research is supported by the EPA grant 2008-ET-MS-3-S2 and the SFI under Grants No. 07/SRC/B1160 and 08/RFP/CHE1349, the Netherlands Organisation for Scientific Research through a VIDI grant (WRB) and the German Research Association (DFG SFB 583, SR and GRK 1626; MPG).

## References

1 (*a*) P. Chen and T. J. Meyer, *Chem. Rev.*, 1998, **98**, 1439; (*b*) B. S. Brunschwig, C. Creutz and N. Sutin, *Chem. Soc. Rev.*, 2002, **31**, 168; (*c*) K. D. Demadis, C. M. Hartshorn and T. J. Meyer, *Chem. Rev.*, 2001, **101**, 2655; (*d*) W. R. Browne, R. Hage and J. G. Vos, *Coord. Chem. Rev.*, 2006, **250**, 1653; (*e*) J. G. Vos and J. M. Kelly, *Dalton Trans.*, 2006, 4869; (*f*) W. R. Browne, N. M. O'Boyle, J. J. McGarvey and J. G. Vos, *Chem. Soc. Rev.*, 2005, **34**, 641.

2 (*a*) S. Rau, B. Schäfer, D. Gleich, E. Anders, M. Rudolph, M. Friedrich, H. Görls, W. Henry and J. G. Vos, *Angew. Chem., Int. Ed.*, 2006, **45**, 6215; (*b*) S. Rau, D. Walther and J. G. Vos, *Dalton Trans.*, 2007, 915; (*c*) H. Ozawa and K. Sakai, *Chem. Commun.*, 2011, **47**, 2227.

3 (*a*) H. Ozawa, Y. Yokoyama, M. Haga and K. Sakai, *Dalton Trans.*, 2007, 1197; (*b*) S. A. Arachchige, J. Brown and K. J. Brewer, *J. Photochem. Photobiol., A*, 2008, **197**, 13; (*c*) E. D. Cline, S. E. Adamson and S. Bernhard, *Inorg. Chem.*, 2008, **47**, 10378; (*d*) P. W. Du, K. Knowles and R. Eisenberg, *J. Am. Chem. Soc.*, 2008, **130**, 12576; (*e*) A. Fihri, V. Artero, M. Razavet, C. Baffert, W. Leibl and M. Fontecave, *Angew. Chem., Int. Ed.*, 2008, **47**, 564; (*f*) C. Li, M. Wang, J. X. Pan, P. Zhang, R. Zhang and L. C. Sun, *J. Organomet. Chem.*, 2009, **694**, 2814; (*g*) Y. Miyake, K. Nakajima, K. Sasaki, R. Saito, H. Nakanishi and Y. Nishibayashi, *Organometallics*, 2009, **28**, 5240; (*h*) B. Probst, C. Kolano, P. Hamm and R. Alberto, *Inorg. Chem.*, 2009, **48**, 1836; (*i*) M. Schulz, M. Karnahl, M. Schwalbe and J. G. Vos, *Coord. Chem. Rev.*, 2012, **256**, 1682; (*j*) S. Soman, G. Singh Bindra, A. Paul, R. Groarke, J. C. Manton, F. M. Connaughton, M. Schultz, D. Dini, C. Long, M. T. Pryce and J. G. Vos, *Dalton Trans.*, 2012, DOI: 10.1039/c2dt32028b.

4 G. Singh Bindra, M. Schulz, A. Paul, S. Soman, R. Groarke, J. Inglis, M. T. Pryce, W. R. Browne, S. Rau, B. J. Maclean and J. G. Vos, *Dalton Trans.*, 2011, **40**, 10812.

5 (*a*) V. N. Kozhevnikov, D. N. Kozhevnikov, O. V. Shabunina, V. L. Rusinov and O. N. Chupakhin, *Tetrahedron Lett.*, 2005, **46**, 1791; (*b*) V. N. Kozhevnikov, O. V. Shabunina, D. S. Kopchuk, M. M. Ustinova, B. König and D. N. Kozhevnikov, *Tetrahedron*, 2008, **64**, 8963.

6 C. J. Mathews, P. J. Smith and T. Welton, *J. Mol. Catal. A: Chem.*, 2004, **214**, 27.

7 W. R. Browne, C. M. O'Connor, J. S. Killeen, A. L. Guckian, M. Burke, P. James, M. Burke and J. G. Vos, *Inorg. Chem.*, 2002, **41**, 4245.

8 K. Sakai, H. Ozawa, H. Yamada, T. Tsubomura, M. Hara, A. Higuchi and M. Haga, *Dalton Trans.*, 2006, 3300–3305.

9 (*a*) L. Cassidy, S. Horn, L. Cleary, Y. Halpin, W. R. Browne and J. G. Vos, *Dalton Trans.*, 2009, 3923; (*b*) Y. Halpin, L. Cleary, L. Cassidy, S. Horne, D. Dini, W. R. Browne and J. G. Vos, *Dalton Trans.*, 2009, 4146.

10 (*a*) P. Du, J. Schneider, L. Fan, W. Zhao, U. Patel, F. N. Castellano and R. Eisenberg, *J. Am. Chem. Soc.*, 2008, **130**, 5056; (*b*) P. Lei,

 

M. Hedlund, R. Lomoth, H. Rensmo, O. Johansson and L. Hammarström, *J. Am. Chem. Soc.*, 2008, **130**, 26.
11 (*a*) R. Baba, S. Nakabayashi, A. Fujishima and K. Honda, *J. Phys. Chem.*, 1985, **89**, 1902; (*b*) D. R. Anton and R. H. Crabtree, *Organometallics*, 1983, **2**, 855.
12 H. Ozawa, M. Haga and K. Sakai, *J. Am. Chem. Soc.*, 2006, **128**, 4926.
13 X. Wang, K. Maeda, A. Thomas, K. Takanabe, G. Xin, J. M. Carlsson, K. Domen and M. Antonietti, *Nat. Mater.*, 2009, **8**, 76.
14 S. Tschierlei, M. Karnahl, M. Presselt, B. Dietzek, J. Guthmüller, L. Gonzalez, M. Schmitt, S. Rau and J. Popp, *Angew. Chem., Int. Ed.*, 2010, **49**, 3981.
15 (*a*) J. R. Ferraro and K. Nakamoto, *Introductory Raman Spectroscopy*, Academic Press Limited, London, 1994; (*b*) D. F. Morris and W. H. Woodruff, in *Spectroscopy of Inorganic Based Materials*, ed. R. J. H. Clark and R. E. Hester, John Wiley & Sons, New York, 1987; (*c*) D. P. Strommen and K. Nakamoto, *J. Chem. Educ.*, 1977, **54**, 474; (*d*) W. R. Browne, N. M. O'Boyle, J. J. McGarvey and J. G. Vos, *Chem. Soc. Rev.*, 2005, **34**, 641.
16 (*a*) P. J. Carroll and L. E. Brus, *J. Am. Chem. Soc.*, 1987, **109**, 7613; (*b*) C. Kumar, J. Barton, I. Gould, N. Turro and J. van Houten, *Inorg. Chem.*, 1988, **27**, 648; (*c*) C. Kumar, J. Barton, I. Gould and N. Turro, *Inorg. Chem.*, 1987, **26**, 1455; (*d*) S. E. J. Bell, *Analyst*, 1996, **121**, 107R; (*e*) J. J. McGarvey, P. Callaghan, C. G. Coates, J. R. Schoonover, J. M. Kelly, L. Jacquet and K. C. Gordon, *J. Phys. Chem. B*, 1998, **102**, 5941; (*f*) C. G. Coates, T. E. Keyes, H. P. Hughes, P. M. Jayaweera, J. J. McGarvey and J. G. Vos, *J. Phys. Chem. A*, 1998, **102**, 5013.
17 (*a*) D. P. Strommen, P. K. Mallick, G. D. Danzer, R. S. Lumpkin and J. R. Kincaid, *J. Phys. Chem.*, 1990, **94**, 1357; (*b*) R. F. Dallinger and W. H. Woodruff, *J. Am. Chem. Soc.*, 1979, **101**, 4391.
18 Y. Zhao and D. G. Truhlar, *Theor. Chem. Acc.*, 2008, **120**, 215.
19 M. Biner, H. B. Buergi, A. Ludi and C. Roehr, *J. Am. Chem. Soc.*, 1992, **114**, 5197.
20 J. E. Bercaw, A. C. Durrell, H. B. Gray, J. C. Green, N. Hazari, J. A. Labinger and J. R. Winkler, *Inorg. Chem.*, 2010, **49**, 1801.
21 A. Draksharapu, Q. Li, H. Logtenberg, T. A. van den Berg, A. Meetsma, J. S. Killeen, B. L. Feringa, R. Hage, G. Roelfes and W. R. Browne, *Inorg. Chem.*, 2012, **51**, 900.
22 M. J. Frisch, G. W. Trucks, H. B. Schlegel, G. E. Scuseria, M. A. Robb, J. R. Cheeseman, G. Scalmani, V. Barone, B. Mennucci, G. A. Petersson, H. Nakatsuji, M. Caricato, X. Li, H. P. Hratchian, A. F. Izmaylov, J. Bloino, G. Zheng, J. L. Sonnenberg, M. Hada, M. Ehara, K. Toyota, R. Fukuda, J. Hasegawa, M. Ishida, T. Nakajima, Y. Honda, O. Kitao, H. Nakai, T. Vreven, J. A. Montgomery, Jr., J. E. Peralta, F. Ogliaro, M. Bearpark, J. J. Heyd, E. Brothers, K. N. Kudin, V. N. Staroverov, R. Kobayashi, J. Normand, K. Raghavachari, A. Rendell, J. C. Burant, S. S. Iyengar, J. Tomasi, M. Cossi, N. Rega, J. M. Millam, M. Klene, J. E. Knox, J. B. Cross, V. Bakken, C. Adamo, J. Jaramillo, R. Gomperts, R. E. Stratmann, O. Yazyev, A. J. Austin, R. Cammi, C. Pomelli, J. Ochterski, R. L. Martin, K. Morokuma, V. G. Zakrzewski, G. A. Voth, P. Salvador, J. J. Dannenberg, S. Dapprich, A. D. Daniels, O. Farkas, J. B. Foresman, J. V. Ortiz, J. Cioslowski and D. J. Fox, *GAUSSIAN 09 (Revision A.2)*, Gaussian, Inc., Wallingford, CT, 2009.
23 (*a*) X. Cao, *THEOCHEM*, 2002, **581**, 139; (*b*) T. H. Dunning Jr. and P. J. Hay, in *Modern Theoretical Chemistry*, ed. H. F. Schaefer III, Plenum, New York, 1976, vol. 3, pp. 1–28; (*c*) D. Andrae, U. Haussermann, M. Dolg, H. Stoll and H. Preuss, *Theor. Chim. Acta*, 1990, **77**, 123.
24 J. Tomasi, B. Mennucci and R. Cammi, *Chem. Rev.*, 2005, **105**, 2999.
25 N. M. O'Boyle, A. L. Tenderholt and K. M. Langner, *J. Comput. Chem.*, 2008, **29**, 839.